Received: 30 March 2021 | Revised: 7 May 2021 | Accepted: 20 May 2021

DOI: 10.1002/pol.20210213

RESEARCH ARTICLE

JOURNAL OF POLYMER SCIENCE WILEY

Chain dynamics in partially cross-linked polyethylene by combined rheology and NMR-based molecular rheology

Farhad Shahsavan[1] | **Mario Beiner**[2,3] | **Kay Saalwächter**[1]

[1]Institut für Physik-NMR, Martin-Luther-Universität Halle-Wittenberg, Halle, Germany

[2]Institut für Chemie, Martin-Luther-Universität Halle-Wittenberg, Halle, Germany

[3]Fraunhofer-Institut für Mikrostruktur von Werkstoffen und Systemen IMWS, Halle, Germany

Correspondence
Kay Saalwächter, Institut für Physik-NMR, Martin-Luther-Universität Halle-Wittenberg, Halle 06120, Germany.
Email: kay.saalwaechter@physik.uni-halle.de

[Correction added on 19-July 2021, after first online publication.]

Abstract

In recent years, ^{1}H double-quantum NMR (DQ NMR) was established as a suitable molecular-rheology technique to elucidate chain dynamics and to determine entanglement or crosslink densities in linear entangled polymer melts and permanent as well as transient networks. In this work, industrial grade high-density polyethylene, partially cross-linked via electron beam irradiation in the semicrystalline state, is probed in the melt state by low-field DQ NMR and shear rheology. The DQ NMR data is analyzed by two approaches, one assuming the presence of a permanent network and the other considering the potentially complex relaxation spectrum of the studied inhomogeneous systems. A correlation between the DQ NMR results and extent of cross-linking is found. By direct comparison of the rheological results and the NMR-based segmental orientation autocorrelation functions (OACF) via time–temperature superposition (TTS), qualitative consistency between the microscopic and macroscopic observables is established. In this way, the frequency range of shear rheology can be extended by about two decades into the 10 krad/s range. The NMR method is thus a valuable extension of the toolbox of characterization techniques, where gel content measurements by solvent extraction proved to be the least sensitive.

KEYWORDS

branching, crosslinked polyethylene (XLPE), DQ NMR, entanglements, irradiated polyethylene, molecular rheology, orientation autocorrelation function

1 | INTRODUCTION

Polyethylene (PE) is among the most consumed polymers. Forming cross-links between the polymer chains, to make a three-dimensional network, is one of the most common modification approaches being extensively used in the rubber and the plastic industry. By cross-linking of PE, undesirable hot-flow (flowing of the PE in high-temperature usage) and cold flow (creep) can be prevented, while the final product can also keep its permanent shape and act as a rubber above the melting point or be equipped with shape memory properties. Cross-linking can be performed by using a peroxide agent,[1,2] silane grafting reactions[3,4] or by using the electron-induced reactive process (EIReP).[5,6] The latter is a rather practical and clean approach that can be applied to room-temperature specimens or molded parts. Based on previous studies, electron-beam irradiation in the solid-state

improves the mechanical properties without affecting the morphology of HDPE's crystals.[7] Besides the gel content measurement to probe the efficiency of the cross-linking process,[7,8] swelling tests based on the Flory–Rehner theory[9,10] and mechanical measurements based on the rubber elasticity[8,11] are common approaches to study the network structure of the cross-linked PE. Alternative approaches are definitively of interest here due to safety issues, high effort for standard methods and limitations regarding the precision of the obtained parameters.

In addition to the mentioned methods, significant research has been devoted to studying the cross-linking of polymers via dynamic-mechanical measurements. Polymers during cross-linking experience a transition from the liquid to solid state, named gel-point, due to the formation and the growth of molecular clusters. It has been confirmed theoretically[12–15] and experimentally[16–18] that the rheological properties around the gel point are best described by power laws. At the gel point of a low-molecular system, the storage and the loss moduli follow a common power-law decay in the low angular frequency (G', $G'' \sim \omega^n$) and tan δ should be unity. Previous works revealed that there is no universality feature concerning the power laws in the case of high molecular weight precursors (entangled polymers).[19] The relaxation exponent is constant at the gel point[20] and after gelation increases with the extent of the cross-linking reaction.[21]

Beyond the macroscopic properties, cross-linking can be probed in terms of the molecular dynamics via solid-state NMR, which is used widely in studying molecular structure and dynamics. One of the first studies on chain dynamics of chemically cross-linked PE is due to Jurkiewicz and et al.[22] measuring the proton spin–lattice relaxation time. However, his method is indirect as it informs only about changes in the overall time scale of fast segmental fluctuations (α process). For a more direct study of chain motions, the orientation dependent nature of the dipolar coupling interaction between the many protons provides access to the anisotropy of segmental motions of the restricted polymer chains. Fast anisotropic motions lead to an averaged residual dipolar coupling (D_{res}) that is proportional to the inverse of the restricted chain length.[23,24] D_{res} can be measured most quantitatively via time-domain double-quantum (DQ) NMR, and even its distribution has been assessed for studying of the network structure in the rubbers.[25] More general investigations have been performed via extracting the segmental dynamics in terms of the orientation autocorrelation function (OACF) of the second Legendre polynomial $C(t) = 5 < P_2(\cos\theta[t+\tau])P_2(\cos\theta(t))>$, where θ is the instantaneous segmental orientation with respect to the magnetic field, for the cases of monodisperse polymer melts[26–29] and transient networks.[30,31] In the former case, a good adherence to predictions of the tube-reptation model could be confirmed, including the expected corrections due to constraint release (CR) and contour length fluctuations (CLF).

This work is motivated by the need for a microscopic access to the chain dynamics in the particularly complex case of partially cross-linked PE, for which we apply DQ NMR for the first time. We intend to introduce DQ NMR as the molecular rheology tool of choice, establishing a consistency between DQ NMR results and rheological data. The results of this research can be used to replace the classical experiments relying on hazardous solvents handled at high temperatures, such as gel content and swelling tests. We note that our time-domain NMR technique can be performed on simple and cost-efficient low-field NMR instruments.

2 | METHODOLOGICAL BACKGROUND

2.1 | NMR spectroscopy

DQ NMR provides a method for quantifying the anisotropic motions of the polymer chains caused by the spatial constraints, that is, entanglements and cross-links. The anisotropic dynamics lead to a residual dipolar coupling (RDC) which is proportional to the local order parameter and consequently to the density of the spatial constrains.

$$S_b = k\frac{D_{res}}{D_{stat}} = \frac{3}{5}\frac{1}{N} \tag{1}$$

Here, D_{res} is the RDC and N is number of the segments between two constraints. Since N^{-1} is proportional to the density of cross-links, we have $D_{res} \propto G'$ in the rubbery plateau.

By a suitable phase cycling in the pulse sequence, two signals are provided in DQ NMR, which are the reference signal (I_{ref}) and the double-quantum signal (I_{DQ}), both as a function of DQ evolution time. The multiple-quantum (MQ) sum signal $I_{\Sigma MQ} = I_{ref} + I_{DQ}$ reflects the transverse relaxation of the coupled protons (corresponding to anisotropic segmental motion) and also a slowly relaxing tail due to uncoupled protons (corresponding to isotropic segmental motion), while I_{DQ} features an intensity build-up signal which is governed by the D_{res}, as well as transverse relaxation from coupled protons only. In a polymeric network, the dangling chains, sol chains and loops are the source of the uncoupled protons signal. As the transverse relaxation effects of coupled protons are the same in both signals in the case of well-developed elastomers, the relaxation effect can in this case be removed via point by point normalization using the ΣMQ

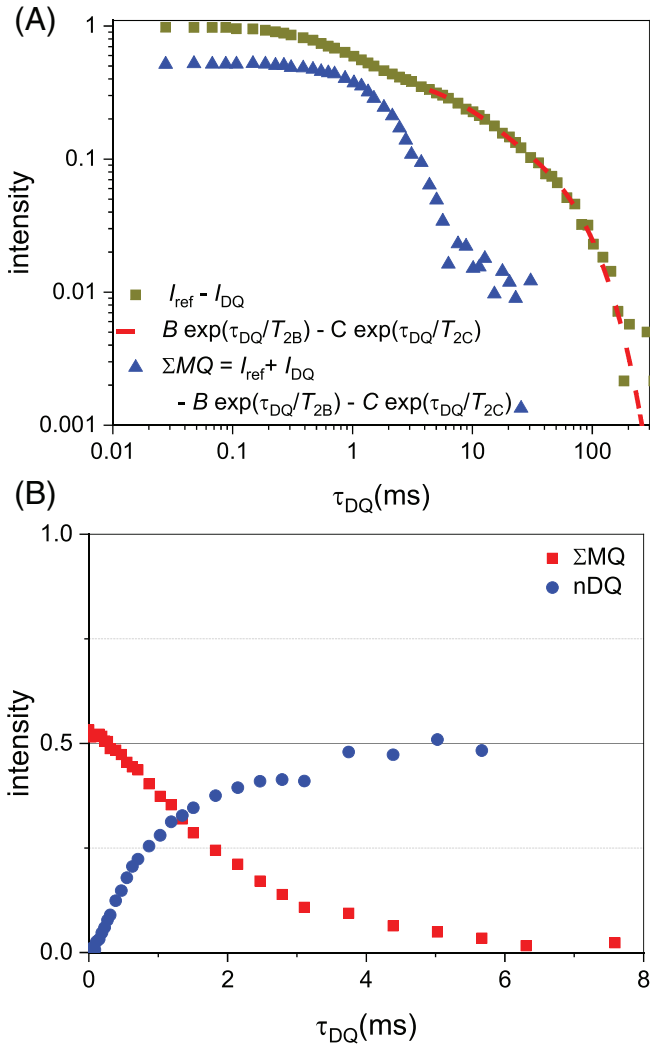

FIGURE 1 Experimental data points for x-HDPE-4 at 160°C. (A) ΔMQ and tail subtracted ΣMQ signals plotted in logarithmic scale, and (B) nDQ buildup and the $I_{\Sigma MQ}$ decay

signal decay function. Before that, it is necessary to subtract the contribution of the uncoupled protons (tails) from the reference signal.[32]

$$I_{nDQ} = \frac{I_{DQ}}{I_{ref} + I_{DQ} - A\exp\left(-\frac{\tau_{DQ}}{T_2^*}\right)} \tag{2}$$

Here A and T_2^* are the fraction and the relaxation time of isotropic moiety, respectively. Tail subtraction is most reliably performed on the difference quantity $I_{\Delta MQ} = I_{ref} - I_{DQ}$.[32] Usually in the case of a well-developed network, the I_{nDQ} build up curve reaches a long-time limiting value of 0.5 after the normalization. In Figure 1 the tail subtraction and the normalized I_{nDQ} is shown. As can be seen the buildup curve has not reached to 0.5 which may be due to the existence of isotropic moieties with the same relaxation time as the network-like protons.

In such cases, simultaneous fitting of the DQ and ΣMQ signals with an exponential decay for transverse relaxation is an alternative approach, as first presented by Lange and et.al[33]:

$$I_{DQ}(\tau_{DQ}) = \frac{1}{2}\sum_{i=1}^{3} a_i\left[1 - \exp\left(-\left(0.378.2\pi D_{res}^{i}\tau_{DQ}\right)^{1.5}\right)\right.$$
$$\left.\times\cos\left(0.583.2\pi D_{res}^{i}\tau_{DQ}\right)\right]\exp\left[-\left(\frac{\tau_{DQ}}{T_{2i}}\right)^{\beta_i}\right] \tag{3}$$

$$I_{\Sigma MQ}(\tau_{DQ}) = \sum_{i=1}^{3} a_i \exp\left[-\left(\frac{\tau_{DQ}}{T_{2i}}\right)^{\beta_i}\right] \tag{4}$$

Here, i represents the moieties, a_i, τ_{DQ} and T_{2i} are the fractions, the DQ evolution times and the transverse relaxation time respectively. This fitting function is based on the empirical Abragam-like (A-L) function which was used for homogeneous networks previously.[25] This function was suitable for fitting the nDQ of the rubber networks far above T_g.

For a more adequate access to the actual chain dynamics in not well-developed networks, an analytical fitting function based on the OACF named the Anderson-Weiss power-law (AWPL) model is applied.[28,34] The OACF describes the fraction of segments which remain in the same orientation after some time t. By assuming a power-law decay for $C(t)$ in the fitted interval,

$$C(t) = \begin{cases} S_b^2 & for\ |t| < t_0 \\ S_b^2\,(t/t_0)^{-\kappa} & for\ |t| \geq t_0 \end{cases}, \tag{5}$$

the following functions can be written:

$$I_{DQ} = \exp\left\{-\frac{\frac{1}{5}D_{res}^2}{(\kappa-2)(\kappa-1)}\left((\kappa-\kappa^2)t_0^2 + (2\kappa^2-4\kappa)\tau_{DQ}t_0 + 2\tau_{DQ}^{2-\kappa}t_0^{\kappa}\right)\right\}$$
$$\times\sinh\left\{\frac{\frac{1}{5}D_{res}^2}{2(\kappa-2)(\kappa-1)}\left((\kappa^2-\kappa)t_0^2 + (2^{3-\kappa}-4)\tau_{DQ}^{2-\kappa}t_0^{\kappa}\right)\right\} \times \exp\left(-\frac{\tau_{DQ}}{T_2}\right) \tag{6}$$

$$I_{\Sigma MQ} = \exp\left\{ -\frac{\frac{1}{5}D_{res}^2}{(\kappa-2)(\kappa-1)} \left(\frac{3}{2}(\kappa-\kappa^2)t_0^2 + (2\kappa^2-4\kappa) \right.\right.$$
$$\left.\left. \tau_{DQ}t_0 + (4-2^{2-\kappa})\tau_{DQ}^{2-\kappa}t_0^{\kappa}) \right\} \times \exp\left(-\frac{\tau_{DQ}}{T_2}\right) \quad (7)$$

Here $S_b \sim D_{res}$ defines the amplitude of $C(t_0)$ ($C(t) \sim D_{res}^2$) at the lower end of the fitted interval and κ is the power-law exponent of the OACF (More details can be found in Ref. 34).

In order to extract the information corresponding to the inhomogeneity of the network structure, one can use a log-normal distribution for D_{res}:

$$P(\ln(D_{res})) = \frac{1}{\sigma_{\ln}\sqrt{2\pi}} \exp\left[\frac{-(\ln(D_{res}) - \ln(D_{med}))^2}{2\sigma_{\ln}^2} \right] \quad (8)$$

The probability distribution depends on the median D_{res} value and the dimensionless distribution width σ. Finally, by numerical integration over the distribution, the fitting function is calculated:

$$I_{nDQ}(\tau_{DQ}) = \int P(\ln(D_{res}))\, I_{nDQ}(\tau_{DQ}, D_{res})\, dln(D_{res}) \quad (9)$$

In Figure 2 the simultaneous fits of the DQ and ΣMQ signals and the fitting ranges are shown for both models. In order to account for the validity limit of AW theory,[34] in AWPL the DQ signal was fitted until the maximum DQ signal. In contrast, for the A-L model the fitting range is extended to the time when the DQ signal has decayed to 20% of its maximum intensity, because this model is not subject to a theory-related validity limit. For both models the ΣMQ signal is fitted over the entire time range, as the AW theory prediction is expected to work well for this relaxation-only signal without dipolar-evolution contributions. Moreover, fitting the entire range is necessary because the signal tails are included in these fits (i.e., we use no separate tail subtraction).

2.2 | Molecular rheology by NMR

To illustrate the relation between the NMR-based OACF and rheological variables, we compare in Figure 3 the time scaling behavior of the OACF and the segmental mean-square displacement (MSD) across the dynamic regimes of the tube model of entangled polymer melts.[35] These quantities are all fundamentally related.[27,35–40] In the Rouse regime I at short times,[35] the MSD scaling exponent of 1/2 is related to the same exponent for the frequency dependence of the storage modulus $G' \sim \omega^{1/2}$ while it is the negative double value for the OACF.[38–40]

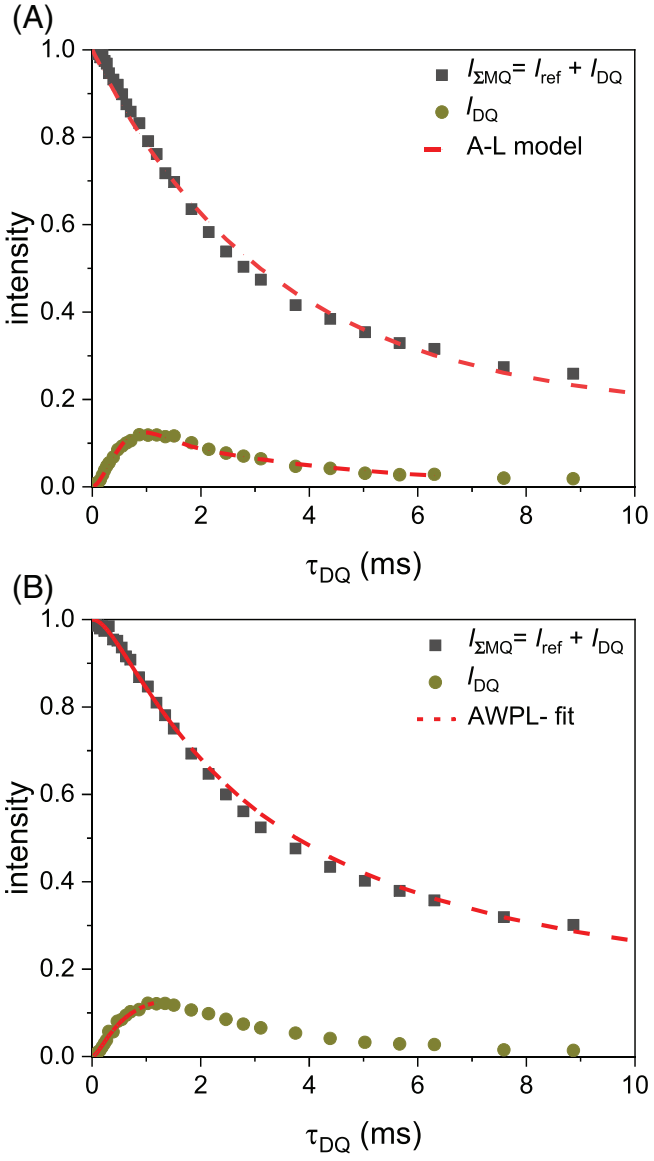

FIGURE 2 Simultaneous fitting of the DQ-NMR signals with (A) the A-L function and (B) the AWPL model

In the longer-time regimes, the time scaling exponents of the OACF and the MSD have a simple inverse relationship, as arising from classical return-to-origin probability arguments used in the theoretical approaches.[35–37] In contrast, G' shows an extended plateau before terminal relaxation because in regimes II and III the chain does not yet leave its tube constraints. Only G'' shows distinct power laws.[41] So although the OACF and the complex modulus are intimately related, there is no simple relation but a qualitative correspondence, with a slowly decaying regime instead of a plateau in NMR.

However, for a well-developed polymer network, the power-law exponent for the OACF is close to zero at longer times beyond the Rouse regime, corresponding to

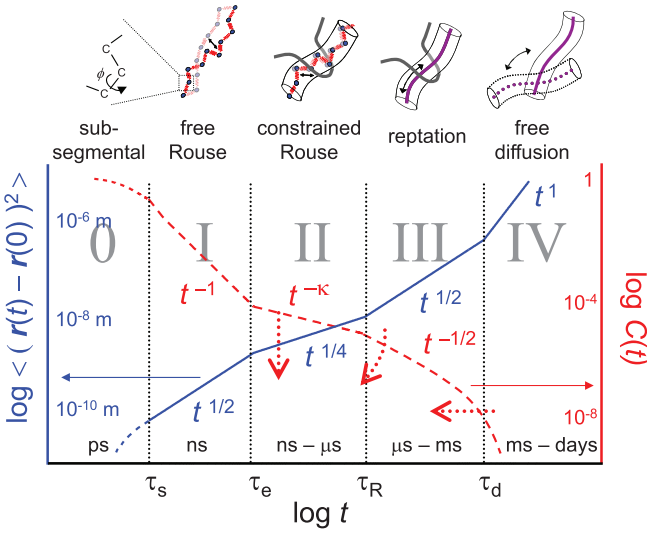

FIGURE 3 The prediction of dynamic regimes by the tube model for the mean-square displacement of segments and the OACF, $C(t)$. In the constrained rouse regime the NMR-detected exponent κ has a limiting value of ¼, but CR was shown lead to larger values $\kappa > 1/4$, dependent on molecular weight.[26] Red dotted arrows indicate trends expected from the admixture of lower-molecular components and defects in inhomogeneous samples. Reproduced from ref. 27, see https://pubs.acs.org/doi/abs/10.1021/ma1025708. Reproduction requires permission of the ACS

the finite plateau modulus. In this regime, Equation (1) holds and for a fixed frequency or time in the plateau range, and we have $G' \sim C(t_{pl})^{1/2} \sim D_{res}$, as proven in numerous works.[42] In the following, our NMR-rheology comparison will focus on the transition from the Rouse to the plateau regime, where systematic changes in the OACF amplitude and the scaling exponents related to the significant polydispersity and the gelation process are expected and observed, and a theoretical connection is missing. However, we can check whether the square-root relation between G' and the OACF, which is valid in both the Rouse and the plateau regimes, may hold qualitatively also in this more complex case. The response is expected to be significantly affected by the significant dynamic inhomogeneity related to the coexistence of low- and high-molecular weight linear and branched structures.

3 | EXPERIMENTAL SECTION

3.1 | Materials

High-density polyethylene (Total Lumicene® mPE M5510 EP, density = 0.955 g/ml, M_n = 27,700 g/mol, PDI = 2.8) was used in this work. The electron beam treatment at STERIS-AST (Bitterfeld, Germany), was carried out at room temperature on polymer sheets with thickness of 2.3 mm using their 10 MeV IBA Rhodotron TT200 J116 accelerator. The applied doses varied from 28 to 168 kGy in 28 kGy steps.

3.2 | Characterization

3.2.1 | Gel content

Sol–gel analysis was carried out by IKTR (Weißandt-Gölzau, Germany) to extract the amount of soluble parts in the material. Approximately 250 mg of the sample with 1.5% of stabilizer was kept in boiling xylene for 8 h. After extraction, the sample was dried in vacuum in two steps: 16 h at room temperature and 2 h at 90°C. Two replicates were tested for each sample and the average value was reported. The gel content value was calculated according to:

$$\text{Gel content}\,(\%) = \frac{m_1}{m_0} \times 100\%, \tag{10}$$

where m_1 and m_0 are the sample masses after and before extraction, respectively.

3.2.2 | Rheological measurements

Dynamic shear measurements were performed using Anton Paar MCR 501 rheometer with 8 mm parallel-plate geometry. Frequency sweeps in the range from 0.1 to 100 rad/s are performed on rubbery samples at 190°C well above the melting point of PE.

3.2.3 | ^{1}H DQ-NMR measurements

NMR measurements were done on a Bruker minispec mq20 benchtop spectrometer (B_0 = 0.47 T), with 90° pulse length of 1.6 and a receiver dead time of 15 μs. The sample temperature was controlled using a Bruker BVT 3000 temperature controller with an accuracy of ±0.5 K. The DQ-NMR experiments were conducted using a compensated version[23] of the Baum-Pines pulse sequence[43] to probe the time evolution of the dipolar coupling interaction in HDPE samples.

4 | RESULTS AND DISCUSSION

The crystallinity of HDPE is about 70%, and it is commonly assumed that cross-linking preferentially takes place in the amorphous phase or in the fold surfaces.[7] Since many if not most chains have more than one part

TABLE 1 Irradiation doses and gel contents for the crosslinked HDPEs

Sample	Irradiation dose (KGy)	Gel content (%)
x-HDPE-1	28	<1%
x-HDPE-2	56	40% ± 10%
x-HDPE-3	84	85% ± 1%
x-HDPE-4	112	87% ± 1%
x-HDPE-5	140	92% ± 2%
x-HDPE-6	168	88% ± 1%

residing in the amorphous phase (i.e., tight adjacent reentry is not a predominant motif), crosslinking of the amorphous chains will lead to a network structure after melting. By applying higher irradiation doses, a threshold appears where cross-linking and chain scission reactions are in equilibrium, and beyond this threshold, higher doses effectively result in degradation. This is well supported by the data in Table 1 that summarizes the gel content values and the irradiation doses (the gel content of HDPE-0 was not measured, but it can safely be assumed to be fully soluble). The gel content increases with irradiation dose significantly for the first three samples (28–84 KGy) whereas above 84 KGy the gel content does not show significant changes any more. At 168 KGy a small drop in gel content is observed that may be related to the degradation of the polymer chains.

Frequency-dependent shear data for all samples measured at 190°C (well above the melting point) are collected in Figure 4. We note that experiments at lower temperatures (starting at 140°C), and using time–temperature superposition (TTS) to construct master curves, did not help in expanding our frequency range significantly. The segmental dynamics is only weakly activated at such high temperatures above the nominal T_g, providing less than half a decade of additional data. We therefore chose to focus on isothermal sweeps.

The storage and loss moduli (Figure 4(A)) of the non-crosslinked sample HDPE-0 show typical features which are commonly found in the flow region of polydisperse or grafted samples. Power-law behavior is found in the investigated frequency window, and Newtonian behavior is not yet observed. A transition towards the behavior of a Newtonian liquid is slightly indicated by increasing slopes at the low-frequency limit of our measurements. Expectedly, all irradiated samples show a systematic increase of G' with dose. Note that the gel content results are invariant in this range, that is, they do not reflect the further increase in modulus at all. For the lowest irradiation doses, clear indications for a plateau in G' are absent, and a relatively pronounced decrease in G' occurs with decreasing frequency.

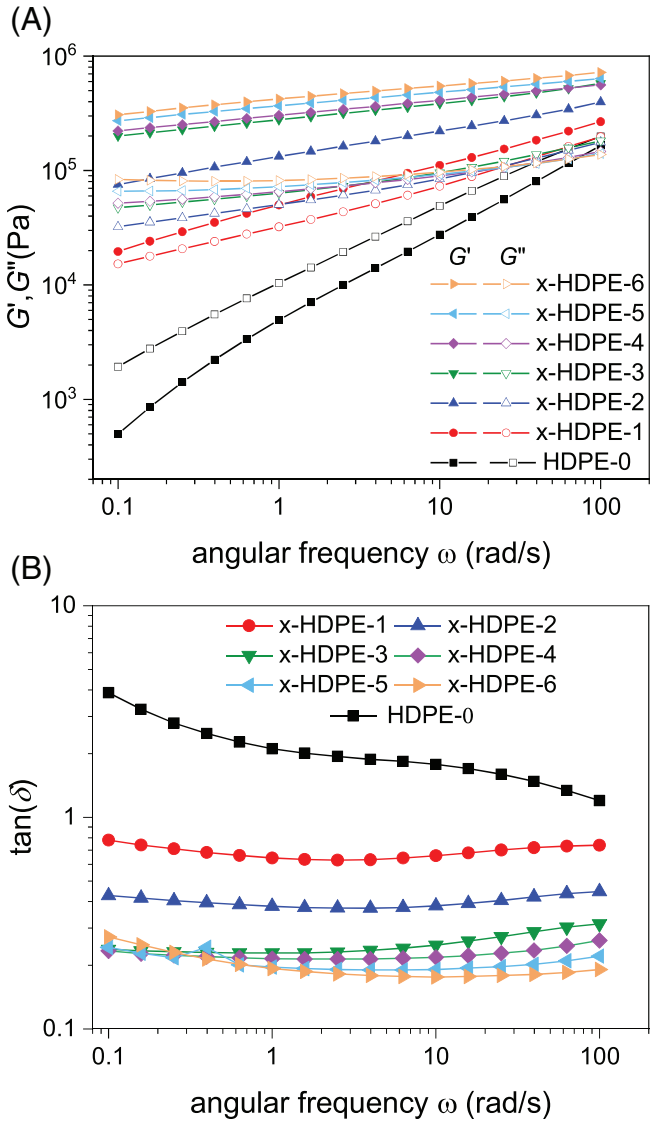

FIGURE 4 Rheological results for all samples; (A) the storage and loss moduli and (B) tan δ plotted versus angular frequency

This trend is significantly reduced but remains present for samples irradiated with higher doses.

Interestingly, in all irradiated samples there is a significant contribution in the loss modulus G''. These values increase with increasing dose while G'' is always smaller than G'. In other words, tan δ is below unity for all irradiated samples in the measured frequency interval (see Figure 4(B)). This may indicate the presence of relaxational contributions related to the sol fraction or slow motions related to long dangling ends. In general, this behavior shows that the investigated samples are by far no perfect polymer networks but show significant imperfections. Due to these it is quite hard to draw conclusions about the irradiation dose needed to form a gel based on shear data alone. The continuous increase of G' and the fact that tan $\delta < 1$ for all irradiated samples highlights

that the number of crosslinks is increasing and that comparative conclusions are possible.

More detailed and reliable information on the gel point and the degree of crosslinking might only be available from extracted samples where the sol fraction is removed. Noticing that tan δ approaches near-constant values near unity in over the whole frequency range for conditions close to sample HDPE-1, together with near-constant power-law exponents for G' and G'', a relation to Winter's criteria for critical gelation seems apparent.[16,17] These features are here amplified by the comparably large-fraction of low-molecular material arising from the polydispersity (and possibly by competing chain scission reactions). Of course, deviations from this phenomenology are expected in the vulcanization (mean-field) universality class,[18,19] which is characterized by an upturn of tan δ (thus the onset of flow) at much lower frequencies outside of our studied range. Based upon the still near-vanishing gel content of sample x-HDPE-1 (see Table 1), it is likely that the gel point is closer to sample x-HDPE-2.

The DQ NMR signals were simultaneously fitted using the A-L function, and the obtained fraction of network like protons and D_{res} are compiled in Figure 5. A finite D_{res} arises as a consequence of anisotropic dynamics of the segments between two physical or chemical spatial or topological constrains. At high temperatures (>170°C), D_{res} increases significantly with the irradiation dose in x-HDPE-3 to 6, whereas for entanglement-dominated x-HDPE-1 and 2 the increase is smaller.

By increasing the temperature, the segments move faster and are able to free themselves from the constraints. This means that an increase in the amount of isotropic moieties (decrease of network-like protons) with temperature is expected, similar to what is observed for HDPE-0 in Figure 5(B). As the irradiation dose increases, not only the fraction of network-like protons is increasing but also its dependency on the temperature is gradually disappearing. Nevertheless, the amount of defects (isotropic moieties) in the network structure is much higher than in well-developed networks. This again demonstrates that our networks are only partially cross-linked, or in the other words, they are diluted with a high amount of defects. It should be noted that the A-L function is well suited for elastomers (being well-developed networks), so by applying it for an imperfect network, weakly coupled protons associated with weakly entangled chains end up to be considered as defects. This explains the high amount of defects in our system obtained with the A-L model. We note that this (apparent) defect fraction is considerably lower than obtained from the extraction experiments (Table 1), since NMR as well as rheology probe transient elasticity in their respective time/frequency windows.

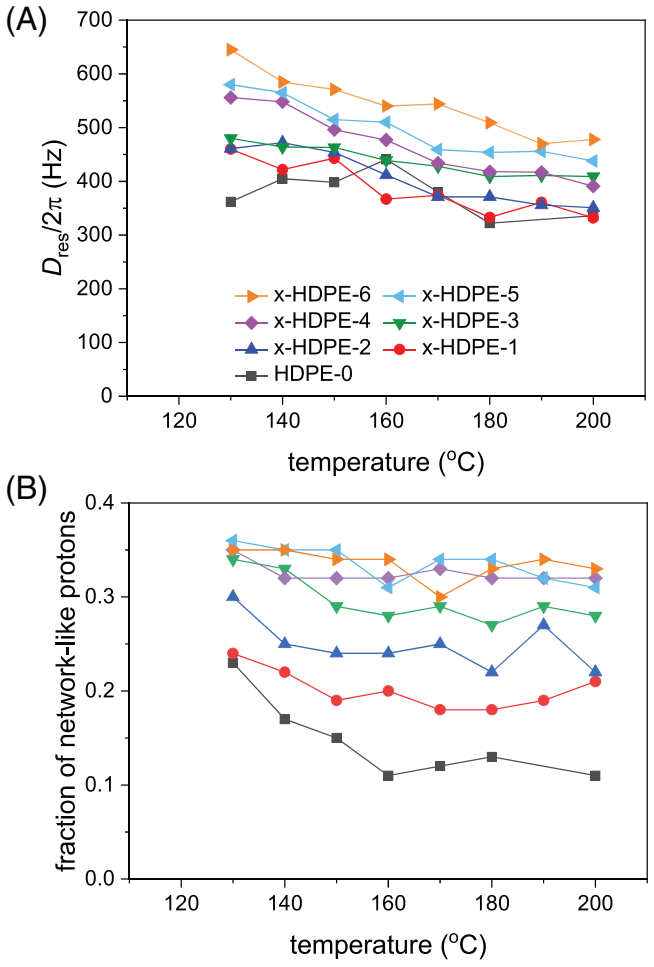

FIGURE 5 (A) RDC and (B) fraction of the network like protons as a function of temperature obtained by simultaneous fitting based upon the A-L function

In Figure 6 the distributions of D_{res} are shown for different irradiation doses at 180°C. Irradiation slightly shifts the median D_{res} to higher values, while for larger D_{res} values a tail starts appearing for the samples with irradiation doses above 84 kGy (x-HDPE-4 to 6). According to the gel content data, x-HDPE-3 is the sample nearest to the equilibrium state between chain scission and cross-linking reactions, and a higher irradiation dose leads to an insignificant increase in gel content value. The D_{res} distribution data reveals that in x-HDPE-4 to 6 with gel content higher than 85%, more irradiation causes an over cross-linking in some parts of the samples.

According to the mentioned results, we stress again that the x-HDPE networks are diluted with a significant amount of defects. Also a significant level of entanglements, some of which are trapped, exist in the network structure and can relax like a polymer melt. Thus, the AWPL model, which is better suited for polymer melts

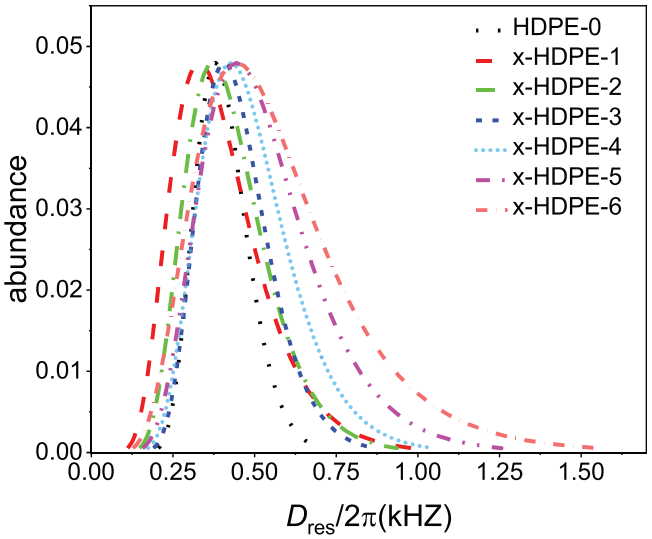

FIGURE 6 Distribution functions of RDCs at 180°C based upon A-L function fitting

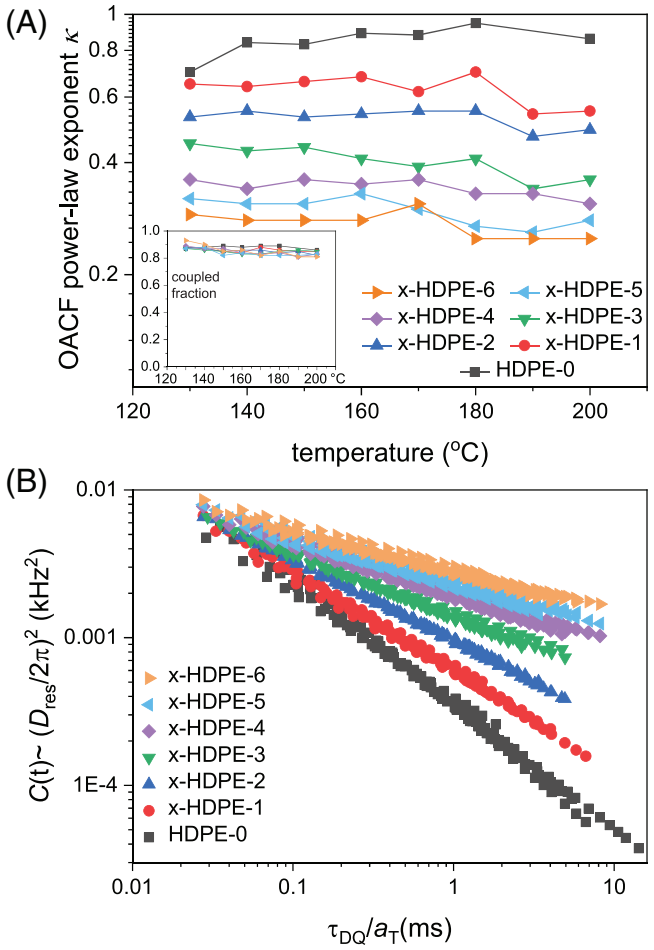

FIGURE 7 (A) Temperature dependence of κ, obtained from AWPL simultaneous fitting for different irradiated samples. The inset shows the fraction of coupled protons from the AWPL model versus temperature. (B) OACF master curves for a reference temperature of 130°C based on the κ and D_{res} values obtained from the AWPL model. The $C(t)$ for different temperatures were shifted using rheological shift factors

and can provide access to the actual shape of the OACF, is now tested for examination of our networks.

Figure 7 shows the results obtained from the AWPL model analysis. In Figure 7(A) the effect of irradiation dose on the chain dynamics is illustrated via the κ values, that is, the power-law exponents of the segmental OACF. The increase of the κ values with the temperature in HDPE-0 reveals a transition to the free-diffusion regime while for the other samples, the dependency of κ on temperature becomes weaker. Unlike the gel content experiment, the κ values sensitively reveal the gradual increase of the cross-links in HDPE-3 to HDPE-6 from the chain-dynamics perspective. Note that this is not at all reflected in the gel content and rheological results. The decrease of κ at high irradiation doses (>84 kGy) confirms this. The inset shows that the fraction of coupled protons varies in a narrow range between 80% and 90% in AWPL model. This means that in all the experiments the OACF is approximately constructed for a fixed fraction of the chains for all temperatures (which is a necessity for TTS) and for all samples (which facilitates the comparison of the data).

Based on the AWPL model and TTS, $C(t)$ was constructed (Figure 7(B)). Even though also here we gain no more than half an additional decade in time by TTS, it is instructive to monitor small changes in the fitted exponent κ, which assumed to be constant and thus represents an average over the fitted time interval. The gel content experiments and rheology revealed that x-HDPE-2 may be nearest to the gel point, and we here confirm that its OACF shows a near-constant log–log slope with an exponent just below the value of 0.5 for reptation motion. Above this line the irradiated polymers are more network-like with the OACF tending towards constrained Rouse motion and ultimately to a plateau. Thus, also from this perspective we find that the gel point is probably located somewhere between x-HDPE-1 and x-HDPE-2. For the three highest irradiated samples (x-HDPE-4,5,6) only a small increase in the OACF and a decrease in κ is observed, which confirms our argument that at higher irradiation doses than 84 kGy, the extents of further cross-linking versus chain scission reactions are practically equal.

In Table 2 key parameters from the DQ NMR and the rheological measurements are summarized. The near-constant coupled fractions were already discussed above. D_{res} follows same monotonic increase as the storage modulus with increasing the irradiation dose. Nevertheless, the most significant discrepancy between the DQ NMR and the rheological measurements appears in the power-law exponents. By comparing κ values and rheological

TABLE 2 DQ NMR and rheological measurement parameters

Sample	Fraction of network-like protons (AWPL)	$D_{res}/2\pi$ (Hz) (at 5 ms)	κ (at 200°C)	Storage modulus (kPa)[a]	Rheological power-law exponent
HDPE-0	0.86	10	0.86	166	0.9[b]
x-HDPE-1	0.85	14	0.55	267	0.37[b]
x-HDPE-2	0.82	20	0.49	397	0.24
x-HDPE-3	0.85	27	0.36	577	0.15
x-HDPE-4	0.83	35	0.31	561	0.13
x-HDPE-5	0.83	38	0.28	636	0.12
x-HDPE-6	0.81	43	0.25	722	0.12

[a]Storage modulus measured at 190°C and 100 rad/s.
[b]Narrow frequency range of 5–100 rad/s.

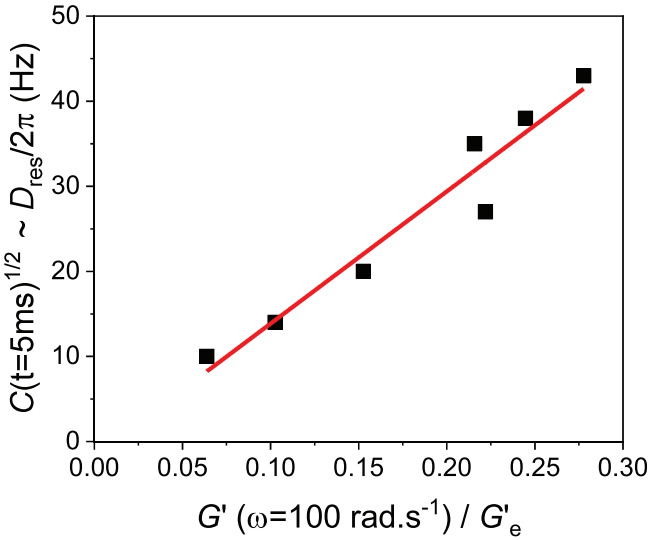

FIGURE 8 D_{res} corresponding to the C(t) at 5 ms versus storage modulus at 100 rad/S divided by the rheological plateau modulus of HDPE for the samples with different irradiation doses

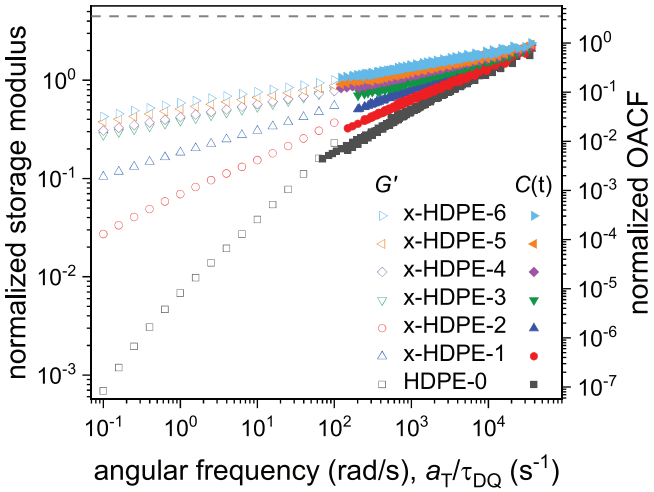

FIGURE 9 Direct comparison of normalized storage modulus and OACF on logarithmic scales. The normalized OACF is plotted versus the inverse DQ evolution time, and its vertical scale is increased by a power of 2 to visually cancel the differences in exponents between NMR and rheology. The dashed line indicates the plateau modulus of PE on the normalized scale

power-law exponents, we observe that in the networks (not HDPE0 and x-HDPE-1), the OACF exponents are about twice higher than the rheological power-law exponents. In polymer melts this is observed for the Rouse regime.[38–40]

To elaborate on the point regarding the absolute values, Figure 8 shows the relation of the square-root of the OACF versus storage modulus at roughly comparable times/frequencies (the dynamic windows do not quite overlap). Gratifyingly, we confirm the offset-free linear relation of the D_{res} with the storage modulus that is well fulfilled and documented for well-entangled melts in the plateau region and well-crosslinked elastomers.[42] This may seem somewhat surprising, considering that the storage moduli are all well below the entanglement-related plateau modulus of PE (G'_e). The finding thus confirms that the relation continues to hold in the Rouse regime.

Figure 9 illustrates a tentative direct comparison of the rheological measurements and the DQ NMR results in terms of the OACF transferred to the frequency domain. We simplistically associate frequency with $1/\tau_{DQ}$, thus inverting the power-law slopes, which corresponds to the results of the actual Fourier transform only in case of a single power-law with constant exponent. By doubling the vertical range of the OACF axis, we consider the factor of 2 difference in exponents. It is nicely demonstrated that the relative decay in normalized G' is continued quite precisely by the normalized $C(t)$. As demonstrated in Figure 8, the G' values are indeed proportional to the square root

of $C(t)$, which is proportional to D_{res} as we observed from Table 2. Since the HDPE-0 data are all in the flow regime, the comparison of the rheology with DQ NMR data is not straightforward in this case and the observed discrepancy in power-law slope is expected (but the rough agreement of the relative magnitudes is still rewarding). By effectively increasing the molecular weight due to the cross-linking, we ensure that the data covers the entanglement plateau and Rouse regimes for the rest of the samples, which obviously enables the direct comparison of the different data sets. Since DQ NMR covers shorter times (thus higher frequencies), the NMR data reflect the upturn into the Rouse regime, subject of course to significant superposition effects in an inhomogeneous sample and with this, a significant "dilution" effect arising from the large fraction of non-entangled defects (short chains and chain ends).

Theoretical treatments of the numerical values of the observed power-law exponents, which characterize a complex mode spectrum, and in particular of the interrelation between frequency-domain and time-domain values probed by rheology and NMR, respectively, are still missing. We believe that the observed relationship will serve as a valuable starting point for further work into this direction.

5 | CONCLUSIONS

In this work, a series of irradiated HDPE were investigated using gel-content determinations, rheology and low-field DQ NMR spectroscopy. It was seen that upon increasing the irradiation dose, chain scission and cross-linking reactions reach an equilibrium leading to a constant extractable fraction, but the degree of cross-linking keeps increasing in the remainder of the sample. Our rheological measurements revealed power-law frequency dependencies of the storage and loss moduli beyond the gel point, as observed previously.

The DQ NMR results were analyzed in two different ways. In a simple 2-component model composed of isotropically mobile parts and a network-like fraction, the data showed that the cross-linking increases the network-like fractions similar to the gel-content results, but with higher sensitivity towards the complex branched architecture, where elastically active inner parts and dangling outer parts are better distinguished. The NMR core observable, the residual coupling characterizing the constraint density on the microscopic level, keeps increasing over the whole sample series.

Using a model better adapted to describing the chain dynamics, the segmental orientation autocorrelation function was constructed on the basis of piecewise constant power laws for all the samples with help of TTS. As the square-root of the correlation function amplitude characterizing the residual coupling was found to be consistent with the high-frequency limiting storage moduli, we could show that DQ NMR data extend the frequency window of rheology by about two decades into the 10 krad/s regime. In the studied range, covering the transition from Rouse dynamics into the developing elastic plateau, we confirm a simple factor of 2 in the NMR-based power-law exponent κ and the rheological counterpart. One core result of practical use is that our low-field time-domain NMR results provided a sensitive, economic and efficient alternative to characterizing the given set of partially cross-linked networks, for which gel content determinations provided practically no distinction in the range of higher irradiation doses.

ACKNOWLEDGMENT

Funding by the European Union (ERDF) is gratefully acknowledged. We thank Herotron E-Beam Service GmbH a STERIS Company (Bitterfeld-Wolfen, Germany) for preparing the irradiated samples and Dr. Albrecht Petzold for help with the rheological experiments.

ORCID

Kay Saalwächter https://orcid.org/0000-0002-6246-4770

REFERENCES

[1] E. M. Kampouris, A. G. Andreopoulos, *J. Appl. Polym. Sci.* **1987**, *34*, 1209.
[2] K. A. Kunert, H. Soszyńska, N. Piślewski, *Polymer* **1981**, *22*, 1355.
[3] M. Narkis, A. Tzur, A. Vaxman, H. G. Fritz, *Polym. Eng. Sci.* **1985**, *25*, 857.
[4] J. R. Atkinson, R. Z. Cicek, *Biomaterials* **1983**, *4*, 267.
[5] R. Salovey, *J. Polym. Sci* **1962**, *61*, 463.
[6] R. J. Yan, Y. Luo, B. Jiang, *J. Appl. Polym. Sci.* **1993**, *47*, 789.
[7] R. Boldt, U. Gohs, U. Wagenknecht, M. Stamm, *Polymer* **2016**, *95*, 1.
[8] H. A. Khonakdar, S. H. Jafari, U. Wagenknecht, D. Jehnichen, *Radiat. Phys. Chem.* **2006**, *75*, 78.
[9] A. Smedberg, T. Hjertberg, B. Gustafsson, *Polymer* **2003**, *44*, 3395.
[10] A. Smedberg, T. Hjertberg, B. Gustafsson, *Polymer* **2004**, *45*, 4867.
[11] H. A. Khonakdar, J. Morshedian, U. Wagenknecht, S. H. Jafari, *Polymer* **2003**, *44*, 4301.
[12] M. Rubinstein, R. H. Colby, Gillmor, JR **1989**. Dynamic scaling for polymer gelation. In: Tanaka F, Doi M, Ohta T (eds) Space–time organization in macromolecular fluids. vol 51. Springer Series in Chemical Physics, pp 66–74, Springer-Verlag, Berlin.
[13] M. Daoud, *J. Phys. A: Math. Theor.* **1988**, *21*, 973.
[14] J. E. Martin, D. Adolf, J. P. Wilcoxon, *Phys. Rev. A* **1989**, *39*, 1325.
[15] H. H. Winter, Evolution of rheology during chemical gelation. in *Permanent and Transient Networks*, Springer, New York. **1987**, p. 104.

[16] H. H. Winter, F. Chambon, *J. Rheol.* **1986**, *30*, 367.
[17] F. Chambon, H. H. Winter, *J. Rheol.* **1987**, *31*, 683.
[18] H. H. Winter, M. Mours, *Adv. Polym. Sci.* **1997**, *134*, 165.
[19] C. P. Lusignan, T. H. Mourey, J. C. Wilson, R. H. Colby, *Phys. Rev. E* **1999**, *60*, 5657.
[20] D. Adolf, J. E. Martin, *Macromolecules* **1990**, *23*, 3700.
[21] M. Mours, H. H. Winter, *Macromolecules* **1996**, *29*, 7221.
[22] A. Jurkiewicz, J. Tritt-Goc, N. Piślewski, K. A. Kunert, *Polymer* **1985**, *26*, 557.
[23] K. Saalwächter, *Prog. Nucl. Magn. Reson. Spectrosc.* **2007**, *51*, 1.
[24] K. Saalwächter, B. Herrero, M. A. López-Manchado, *Macromolecules* **2005**, *38*, 9650.
[25] W. Chassé, J. López Valentín, G. D. Genesky, C. Cohen, K. Saalwächter, *J. Chem. Phys.* **2011**, *134*, 44907.
[26] F. Vaca Chávez, K. Saalwächter, *Phys. Rev. Lett.* **2010**, *104*, 198305.
[27] F. Vaca Chávez, K. Saalwächter, *Macromolecules* **2011**, *44*, 1549.
[28] K. Saalwächter, A. Heuer, *Macromolecules* **2006**, *39*, 3291.
[29] M.-L. Trutschel, A. Mordvinkin, F. Furtado, L. Willner, K. Saalwächter, *Macromolecules* **2018**, *51*, 4108.
[30] A. Mordvinkin, M. Suckow, F. Böhme, R. H. Colby, C. Creton, K. Saalwächter, *Macromolecules* **2019**, *52*, 4169.
[31] A. Mordvinkin, D. Döhler, W. H. Binder, R. H. Colby, K. Saalwächter, *Phys. Rev. Lett.* **2020**, *125*, 127801.
[32] K. Saalwächter, M. Klüppel, H. Luo, H. Schneider, *Appl. Magn. Reson.* **2004**, *27*, 401.
[33] F. Lange, K. Schwenke, M. Kurakazu, Y. Akagi, U. Chung, M. Lang, J.-U. Sommer, T. Sakai, K. Saalwächter, *Macromolecules* **2011**, *44*, 9666.
[34] A. Mordvinkin, K. Saalwächter, *J. Chem. Phys.* **2017**, *146*, 94902.
[35] M. Doi, S. F. Edwards, *The Theory of Polymer Dynamics*, Oxford University Press, Oxford. **1988**.
[36] P. G. de Gennes, *J. Chem. Phys.* **1971**, *55*, 572.
[37] R. C. Ball, P. T. Callaghan, E. T. Samulski, *J. Chem. Phys.* **1997**, *106*, 7352.
[38] R. Kimmich, N. Fatkullin, *Adv. Polym. Sci.* **2004**, *170*, 1.
[39] A. Herrmann, V. N. Novikov, E. A. Rössler, *Macromolecules* **2009**, *42*, 2063.
[40] Z. Wang, A. E. Likhtman, R. G. Larson, *Macromolecules* **2012**, *45*, 3557.
[41] F. Mohamed, M. Flämig, M. Hofmann, L. Heymann, L. Willner, N. Fatkullin, N. Aksel, E. A. Rössler, *J. Chem. Phys.* **2018**, *149*, 44902.
[42] A. Vieyres, R. Pérez-Aparicio, P.-A. Albouy, O. Sanseau, K. Saalwächter, D. R. Long, P. Sotta, *Macromolecules* **2013**, *46*, 889.
[43] J. Baum, A. Pines, *J. Am. Chem. Soc.* **1986**, *108*, 7447.

How to cite this article: F. Shahsavan, M. Beiner, K. Saalwächter, *J Polym Sci* **2021**, 1.
https://doi.org/10.1002/pol.20210213